International Journal of Applied Earth Observation and Geoinformation 120 (2023) 103348

Contents lists available at ScienceDirect

International Journal of Applied Earth Observation and Geoinformation

journal homepage: www.elsevier.com/locate/jag

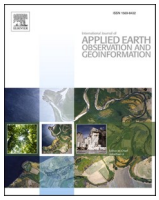

Mapping Eucalyptus plantation in Guangxi, China by using knowledge-based algorithms and PALSAR-2, Sentinel-2, and Landsat images in 2020

Chenchen Zhang [a], Xiangming Xiao [a,*], Liangcheng Zhao [b], Yuanwei Qin [a], Russell Doughty [c], Xinxin Wang [d], Jinwei Dong [f], Xuebin Yang [e]

[a] Department of Microbiology and Plant Biology, Center for Earth Observation and Modeling, University of Oklahoma, Norman, OK 73019, USA
[b] School of Ecology and Nature Conservation, Beijing Forestry University, Beijing 100083, China
[c] College of Atmospheric and Geographic Sciences, University of Oklahoma, Norman, OK 73019, USA
[d] Ministry of Education Key Laboratory for Biodiversity Science and Ecological Engineering, National Observations and Research Station for Wetland Ecosystems of the Yangtze Estuary, Institute of Biodiversity Science and Institute of Eco-Chongming, School of Life Sciences, Fudan University, Shanghai 200438, China
[e] Geography and the Environment Department, Syracuse University, Syracuse, NY 13244, USA
[f] Key Laboratory of Land Surface Pattern and Simulation, Institute of Geographic Sciences and Natural Resources Research, Chinese Academy of Sciences, Beijing 100101, China

ARTICLE INFO

Keywords:
Forest mapping
EVI
Red edge bands
Google Earth Engine

ABSTRACT

Eucalyptus plantations promote the economic development of forestry in southern China, but many studies have reported their negative environmental impacts, such as high water resource usage of certain species of Eucalyptus plants and losses in biodiversity. To date, annual maps of Eucalyptus plantations at large scales with high spatial resolutions are not yet available. Here, we investigated the spectral properties of Eucalyptus plantations and developed a knowledge-based Eucalyptus plantation mapping algorithm. We produced annual maps of Eucalyptus plantation at 10-m spatial resolution in the Guangxi Zhuang Autonomous Region (Guangxi), China, using our proposed algorithm and images of ALOS PALSAR-2, Sentinel-2, and Landsat (ETM+/OLI) in a single year. First, we generated annual evergreen forest maps using PALSAR-2 and Landsat/Sentinel-2-based vegetation index time series data. Second, we distinguished Eucalyptus plantations from the evergreen forest layer using the unique biophysical features of Eucalyptus plantations, the Sentinel-2 red edge bands, and Landsat/Sentinel-2-based enhanced vegetation index (EVI). Our resultant 2020 Eucalyptus plantation map had high producer's, user's, and overall accuracies of 0.85, 0.89, and 0.96, respectively. There were 3.10×10^6 ha of Eucalyptus plantation in Guangxi in 2020. Among the 14 administrative units, Wuzhou City had the largest Eucalyptus plantation area in Guangxi, followed by Nanning, Baise, and Chongzuo cities. We demonstrated the potential of knowledge-based mapping approaches for identifying evergreen forest and Eucalyptus plantations in complex and fragmented landscapes where cloud cover is frequent. Our 10-m Eucalyptus plantation map is the most current dataset available and can be used to assist the sustainable production of Eucalyptus, ecological assessments, and conservation.

1. Introduction

As one of the most planted broadleaf tree species worldwide, Eucalyptus has become the main tree species for fast-growing and productive forests in southern China because of its rapid growth, biomass yield, resistance to disease and pests, tolerance to infertile soil, stem shape, and its wide range of uses (Deng et al., 2020; Zhang and Wang, 2021). Eucalyptus plantations promote the economic development of forestry. For example, they provide wood for charcoal, timber, construction materials, and firewood. In addition, Eucalyptus oil can be used as a cleaning solution and food supplement. However, Eucalyptus growth requires large amounts of nutrients and more water than other alternative plantations in the early growth stage, which may cause environmental damage such as biodiversity loss (Forrester et al., 2006;

* Corresponding author at: Department of Microbiology and Plant Biology, University of Oklahoma, 101 David L. Boren Blvd., Norman, OK 73019, USA.
E-mail address: xiangming.xiao@ou.edu (X. Xiao).

https://doi.org/10.1016/j.jag.2023.103348
Received 16 February 2023; Received in revised form 1 May 2023; Accepted 6 May 2023

White et al., 2022; Zinn et al., 2002). As a result, accurate and timely information on the Eucalyptus plantation area is essential for precise forestry planning and management. However, no maps of Eucalyptus plantations at large scales and high spatial resolutions are publicly available.

During the past few decades, enormous efforts have been devoted to mapping and monitoring forests and plantations, including rubber plantations (Dong et al., 2013; Dong et al., 2012b) and oil palm plantations (Danylo et al., 2021; Dong et al., 2020), at local, regional, and global scales using satellite datasets (Hansen et al., 2013; Qin et al., 2015; Rodríguez et al., 2021). Nevertheless, only a few studies have focused on Eucalyptus plantation identification and mapping (Table 1) in Portugal (Forstmaier et al., 2020; Oliveira et al., 2021), Brazil (Le Maire et al., 2014), Thailand (Huang et al., 2021a), and China (Liang et al., 2017; Lu et al., 2020).

Optical images are the most frequently used data in these Eucalyptus plantation mapping studies, which included very high spatial resolution (VHSR, meters) images, high spatial resolution (HSR, tens of meters) images, and moderate spatial resolution (MSR, hundreds of meters) images. For example, Deng et al. (2020) produced a Eucalyptus plantation map for Guangxi in 2018. They first used a statistical hypothesis test to determine if a pixel belonged to a plantation based on time series EVI data derived from Landsat images between 2013 and 2018. Then they applied broadleaf/needleleaf classification using the red edge and nir infrared (NIR) bands of Sentinel-2 data to distinguish Eucalyptus plantations from coniferous trees including pine and fir. Two studies (De Luca et al., 2022; Huang et al., 2021a) combined optical and synthetic aperture radar (SAR) data to map Eucalyptus plantations, as Sentinel-1 are freely available to the public and provide complementary information to optical images (Table 1). The algorithms used in these studies were all information-based supervised classification methods, which use image data from the regions of interest (ROIs) to train classification algorithms (e.g., support vector machine (SVM), neural networks (NN), decision tree (DT), and random forest (RF)), and then apply the trained algorithms to generate Eucalyptus plantation maps (Chen et al., 2021; Deng et al., 2020; Le Maire et al., 2014; Liang et al., 2017). Information-based algorithms are powerful and efficient tools for generating Eucalyptus plantation maps, but their complexity and opacity make it challenging to comprehend how the models made their final decisions. In addition, these techniques rely on ample high-quality training data and are difficult to be extended to large regions.

The knowledge-based supervised classification approach analyzes time series image data of individual pixels and identifies unique spectral and or microwave characteristics of specific land cover types, such as phenology-based spectral signatures, and utilizes these unique characteristics to identify and map specific land cover types. In contrast to information-based algorithms that require large number of training samples, knowledge-based algorithms, once developed and validated, have the potential to be applied directly to other years or regions without the need for new and large training samples. In recent years, a number of studies have documented the potential and advantages of knowledge-based algorithms to generate maps of rubber plantations (Dong et al., 2013; Dong et al., 2012b), mangrove forests (Chen et al., 2017), paddy rice (Dong et al., 2015; Dong et al., 2016; Xiao et al., 2006; Xiao et al., 2005a), and *Spartina alterniflora* marsh (Zhang et al., 2020b). However, the phenology of Eucalyptus plantations and their unique biophysical features compared to other evergreen species are poorly understood. In addition, the knowledge-based algorithm has not been applied to the identification and mapping of Eucalypts plantations, yet.

Time series Landsat images at 30-m spatial resolution can capture leaf/canopy phenology (LCP) of different tree species and the land surface phenology (LSP) of individual plantation stands. These characteristics are advantageous for plantation mapping as has been demonstrated in several recent studies (Chen et al., 2017; Dong et al., 2013; Pasquarella et al., 2018). However, although Landsat has an 8-day revisit cycle in a bi-satellite system, it is challenging to acquire enough good-quality observations of Landsat to accurately characterize tree phenology in many areas with frequent cloud cover (Griffiths et al., 2019). Since the public release of Sentinel-2 10-m and 20-m data in 2015, several studies have integrated Landsat and Sentinel-2 images to map forests and plantations (Li et al., 2019; Parida and Kumar, 2020; Wang et al., 2022). The Sentinel-2A/B together have 5-day revisit cycle, which increases the amount of good-quality observations in a year and better captures phenological information and changes of the land surface (Wang et al., 2020a). The Sentinel-2 red edge bands and red edge derived indices have aided plantation mapping, including rubber plantations (Xiao et al., 2020), tea plantations (Zhu et al., 2019), and oil palm plantations (Nomura and Mitchard, 2018). However, the potential of red edge bands for tracking and detecting the phenological differences between Eucalyptus plantations and other tree species has not been evaluated.

China is the world's second largest Eucalyptus plantation country, only behind Brazil. As reported by China's 9th National Forest Inventory (NFI) (2014–2018), Guangxi Zhuang Autonomous Region has 47 % of the total area of Eucalyptus plantation in China. It is critical to obtain detailed knowledge of the spatial distribution of Eucalyptus plantations for decision making, research, and ecosystem protection. The objectives of this study were to (1) develop a knowledge-based algorithm to identify and map Eucalyptus plantations by combining Sentinel-2, Landsat, and PALSAR-2, and apply the proposed algorithm to produce Eucalyptus plantation map at 10-m in Guangxi for 2020; (2) explore the potential of the red edge bands of Sentinel-2 for Eucalyptus plantation mapping; and (3) compare and evaluate the proposed Eucalyptus mapping algorithm using the 2018 Eucalyptus datasets from previous studies.

Table 1
A summary of satellite images and algorithms for Eucalyptus plantation mapping.

Methods	Optical image data			Optical + SAR image data (Sentinel-2, Landsat, Sentinel-1, PALSAR)
	VHSR (< 10 m; e.g., ZiYuan, GaoFen)	HSR (10 m–30 m; e.g., Sentinel-2, Landsat)	MSR (250 m–500 m; e.g., MODIS)	
Information-based supervised classification (e.g., NN, DT, SVM, RF)	(Chen et al., 2021; Liang et al., 2017)	(da Costa et al., 2021; Deng et al., 2020; Forstmaier et al., 2020; Lu et al., 2020; Oliveira et al., 2021)	(Le Maire et al., 2014)	(De Luca et al., 2022; Huang et al., 2021a)
Knowledge-based supervised classification				This study

2. Materials and methods

2.1. Study area

Guangxi is located in southern China and comprises 14 cities and prefectures with an area of ~236,700 km^2. The topography of Guangxi is complex with elevation ranging from 0 to 2113 m above sea level (Fig. 1). There are large flat plains in the central and southern parts of Guangxi, surrounded by mountains and hills. Guangxi belongs to a subtropical to tropical climate, where abundant rainfall and warm temperatures provide a good growing environment for plants. According to the report of China's 9th NFI, Guangxi had the third highest forest (arboreal forest, bamboo forest, and shrub) coverage (60.17 %) in China in 2015. Guangxi is China's largest timber production region with a yearly production of ~25 million m^3 (Deng et al., 2020; Zeng et al., 2015). Eucalyptus, pine, and fir are the main timber cultivars in Guangxi

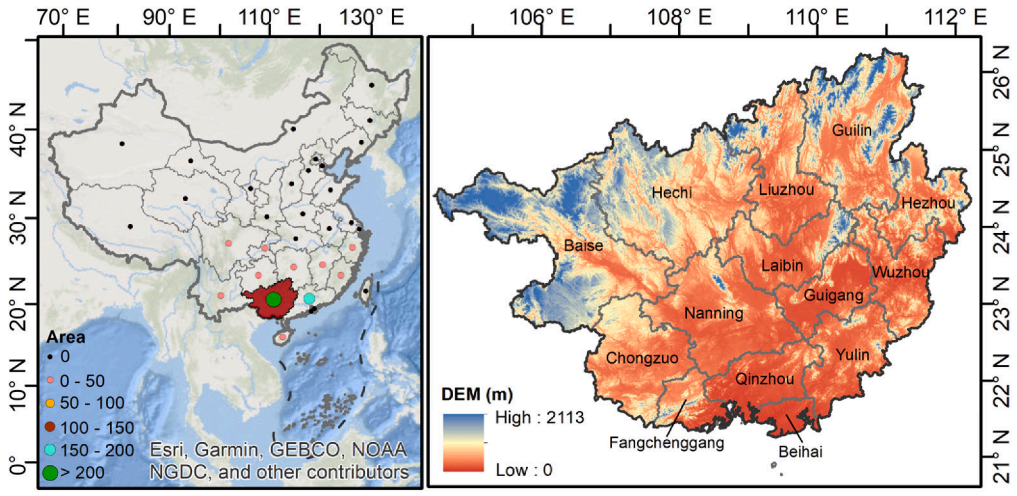

Fig. 1. (a) Eucalyptus plantation area (unit: 10^4 ha) by province and the location of Guangxi and (b) digital elevation model (DEM) of Guangxi. Eucalyptus plantation area by province was reported in China's 9th NFI.

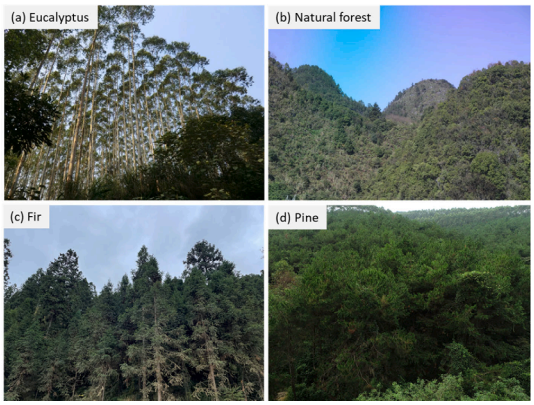

Fig. 2. Field photos of main forest types in Guangxi. Photos of (a) Eucalyptus and (b) natural forest were downloaded from the Global Geo-Referenced Field Photo Library (https://www.ceom.ou.edu/photos/). Photos of (c) fir and (d) pine were provided by Xinya Qin.

(Fig. 2), where Eucalyptus accounts for > 70 % of total timber production (Forestry Bureau of Guangxi, 2018). Both farmers and state-owned forestry companies plant Eucalyptus trees, and thus the size of Eucalyptus plots varies widely from a few to hundreds of hectares.

2.2. Datasets

2.2.1. ALOS PALSAR-2 data

We used 25-m ALOS PALSAR-2 yearly mosaic L-band images from 2018 to 2020 in Google Earth Engine (GEE) (Fig. 3). These mosaic data were selected from the original observations with the least response to surface moisture (Shimada et al., 2014). The PALSAR-2 imagery were ortho-rectified and slope corrected using the 90-m SRTM digital elevation model (DEM). The PALSAR-2 data have two polarizations (HH and HV). The digital number (DN) values in the two polarization bands were converted to gamma naught (γ^0) values in decibel unit (dB) using $\gamma^0 = 10log_{10}(DN^2) - 83$ dB (Shimada et al., 2009). Difference (HH-HV) and ratio (HH/HV) values were calculated. Approximately 4.9×10^6 pixels (1.2 % of the total number of pixels) in Guangxi had no PALSAR-2 data in 2020 (Fig. 3a), and thus the missing data were gap filled with data from 2018 (Fig. 3c, d), as PALSAR-2 data for 2019 in the same pixels were also unavailable (Fig. 3b).

2.2.2. Sentinel-2 data

We used Sentinel-2A/B Level-2A surface reflectance (SR) data from January 1, 2020, to December 31, 2020, and top of atmosphere (TOA) reflectance data from January 1, 2018, to December 31, 2018 as SR data were not available for 2018. Compared to other multi-spectral satellites such as Landsat and MODIS, Sentinel-2 has four additional spectral bands in the red edge region, centering at 704 nm (B5 or RE1), 740 nm (B6 or RE2), 783 nm (B7 or RE3), and 865 nm (B8A or RE4), which are specifically designed to vegetation monitoring (Clevers and Kooistra, 2011), and are reported to be the most important ranking attributes in Sentinel-2 data classification (Sothe et al., 2017). We removed clouds and cloud shadows using cloud mask information within the Quality Assessment (QA60) bitmask band. Spatial distributions of total observation number and good-quality observation number for Sentinel-2 images in 2020 are presented in Fig. 4a, c.

The normalized difference vegetation index (NDVI) (Tucker, 1979), enhanced vegetation index (EVI) (Huete et al., 2002; Huete et al., 1997), and land surface water index (LSWI) (Xiao et al., 2004; Xiao et al., 2005b) were calculated for each image using Eqs. (1)–(3). NDVI and EVI are used to track the seasonal changes of vegetation canopy (Huete et al., 2002; Huete et al., 1997; Tucker, 1979). LSWI is used to monitor the seasonal changes of vegetation and soil water.

$$\mathrm{NDVI} = \frac{NIR - Red}{NIR + Red} \tag{1}$$

$$\mathrm{EVI} = 2.5 \times \frac{NIR - Red}{NIR + 6Red - 7.5Blue + 1} \tag{2}$$

$$\mathrm{LSWI} = \frac{NIR - SWIR}{NIR + SWIR} \tag{3}$$

where *Blue*, *Red*, *NIR*, and *SWIR* are the SR values of blue (496.6 nm), red (664.5 nm), near-infrared (835.1 nm), and shortwave-infrared (1613.7 nm) bands for the Sentinel-2A Multi Spectral Instrument (MSI) sensor.

2.2.3. Landsat data

We used Landsat 7/8 Level-2 SR data in GEE from January 1, 2018, to December 31, 2018, and January 1, 2020, to December 31, 2020. Clouds and cloud shadows were removed using the pixel quality assessment (pixel_qa) band. Spatial distributions of the number of total observations and good-quality observations of Landsat 7/8 images in 2020 are shown in Fig. 4b, d. NDVI, EVI, and LSWI were calculated for each Landsat image (see Eqs. (1)–(3)). The annual maximum NDVI ($\mathrm{NDVI_{max}}$) was calculated by combining NDVI derived from Sentinel-2

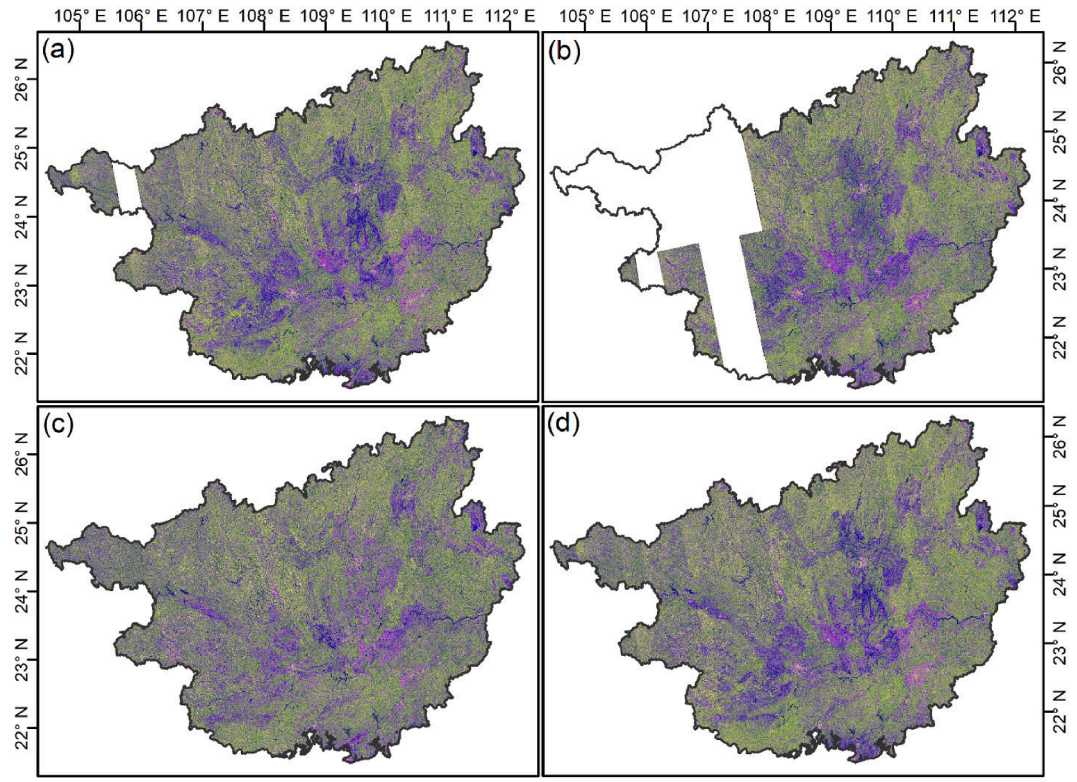

Fig. 3. Spatial distribution of the false-color combinations of PALSAR-2 data (R:G:B = HH:HV: HH-HV) in Guangxi, China. (a)-(c) show PALSAR-2 images for (a) 2020, (b) 2019, and (c) 2018. (d) Gap filled PALSAR-2 images for 2020.

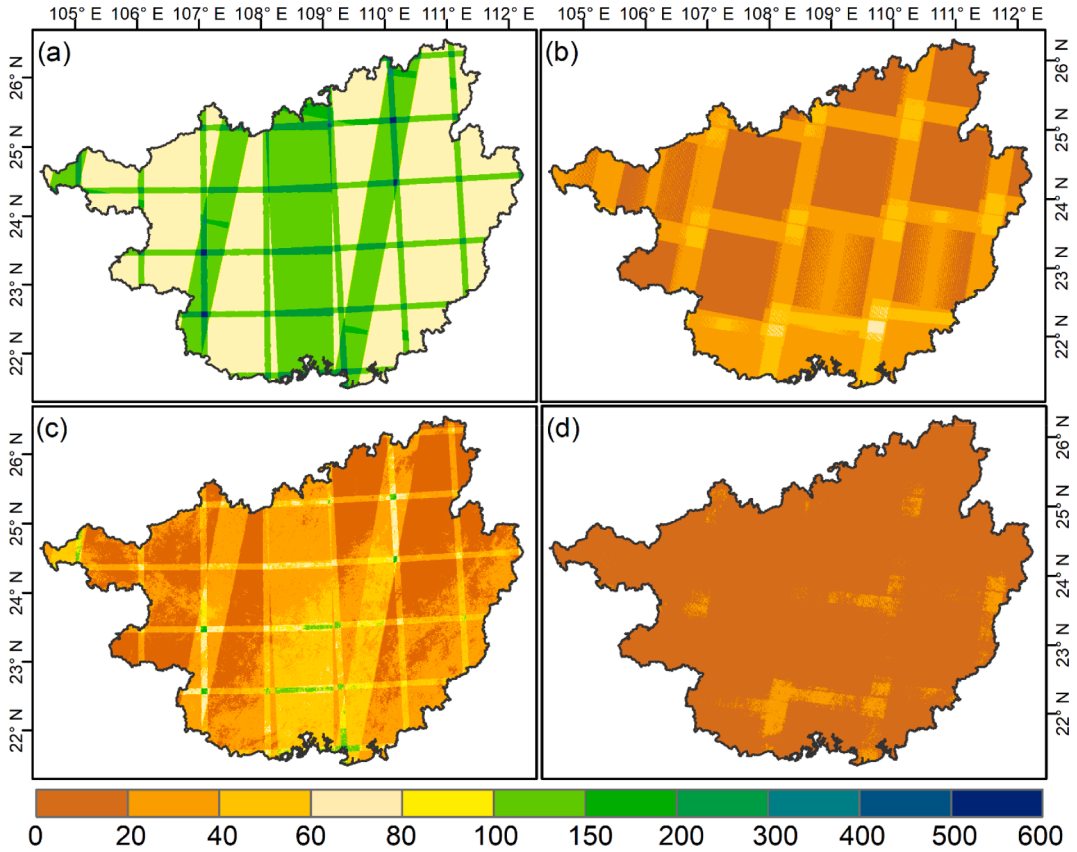

Fig. 4. Spatial distributions of total observation amount of (a) Sentinel-2 and (b) Landsat 7/8, and good-quality observation amount of (c) Sentinel-2 and (d) Landsat 7/8 in 2020.

and Landsat.

2.2.4. Ground reference data

We used VHSR images from Google Earth, geo-referenced field photos, and training samples shared in the literature to collect training samples of different tree species. First, we collected field photos and KML files with coordinates in Guangxi, China, which are hereafter abbreviated to Points of Interest (POIs), from the Global Geo-Referenced Field Photo Library (https://www.ceom.ou.edu/photos/), and geo-linked them to Google Earth. Second, we downloaded different tree species training polygons shared by Deng et al. (2020) as SHP files from https://code.earthengine.google.com/?accept_repo=users/siatsiatns/eucalypt. These polygons included 19 Eucalyptus plantations, 27 fir plantations, 29 pine plantations, and 10 evergreen natural forests, which were obtained by field survey in 2017 and visual identification through VHRS images in Google Earth. Third, we overlaid field photos and shared training polygons with Google Earth VHSR images to collect training samples for Eucalyptus plantations and other evergreen tree species. Finally, we collected polygons for 117 Eucalyptus plantations, 67 natural evergreen forests, 25 fir plantations, and 29 pine plantations for image analysis and algorithm development (Fig. 5a). Of these, 107 Eucalyptus plantations, 67 natural evergreen forests, 8 fir plantations, and 5 pine plantations training samples were collected by combing filed photos and VHSR images. The remaining training samples were obtained and adapted from Deng et al.'s (2020) study.

2.3. Methods

We developed a knowledge-based algorithm and workflow to identify and map the annual maps of Eucalyptus plantations in Guangxi (Fig. 6). We first identified evergreen forest using PALSAR-2 data and Landsat/Sentinel-2-based time-series EVI and LSWI data, and then distinguished Eucalyptus plantation within in the evergreen forest layer using Sentinel-2 red edge bands and Landsat/Sentinel-2-based time series EVI data.

2.3.1. Algorithms to identify forest and evergreen forest

The effective identification of Eucalyptus plantations starts with accurate forest and evergreen forest maps. As defined by the Food and Agricultural Organization (FAO), forest is land with trees above 5-m and a canopy cover of over 10 % (FAO, 2020), and we adopted this definition for our study. L-band PALSAR is able to penetrate clouds, smoke, and haze to capture the structure and aboveground biomass of forests (Imhoff, 1995; Kovacs et al., 2013) and can help distinguish forest from non-forest (Reiche et al., 2016). However, some urban lands may have similar higher backscatter coefficients with forests (Qin et al., 2015). $NDVI_{max}$ has the potential to reduce the commission error caused by urban lands (DeFries and Townshend, 1994). Previous studies have developed a detailed workflow to identify and map forests by combining PALSAR and $NDVI_{max}$, and produced forest maps with high accuracies in China (Qin et al., 2015), Southeast Asia (Dong et al., 2012a), and the United States (Yang et al., 2021). We used the same algorithm for forest cover mapping in China (i.e., $3 < HH\text{-}HV < 7$ & $-15 < HV < -9$ & $0.35 < HH/HV < 0.75$ & $NDVI_{max} \geq 0.5$) (Qin et al., 2015) to generate forest maps for Guangxi.

In previous studies, we developed an evergreen vegetation identification algorithm using time series LSWI and EVI (Dong et al., 2015; Xiao et al., 2009). Here we applied the same algorithm LSWI > 0 and EVI > 0.2 with a frequency of > 90 % (Wang et al., 2020a) to identify evergreen forest in the forest map. The resultant annual evergreen forest maps were used as the baseline map for Eucalyptus plantation identification in the next step.

2.3.2. Phenology analysis of Eucalyptus and other evergreen tree species

Plant traits, including leaf type (broadleaf vs needleleaf), leaf seasonality (evergreen vs deciduous), leaf longevity (one-year vs multiple-year old leaf), leaf size and shape (large vs small; long vs short), and leaf clumping or cluster, differ among trees in natural forests, Eucalyptus, fir, and pine. Eucalyptus leaves are evergreen broadleaves which are narrow and thin. Leaves of trees in natural forests are large and thick evergreen broadleaves. Fir and pine leaves are evergreen needleleaves. Compared to other evergreen tree species in Guangxi, Eucalyptus has several unique phenological features in terms of leaf longevity, leaf area index (LAI), and leaf growth rate. We collected the information about leaf longevity and LAI from the Plant Trait Database (https://www.try-db.org/TryWeb/Data.php) and publications (DeRose and Seymour, 2010; Mthembu, 2001; Rody et al., 2014; Yan et al., 2019; Zhao et al., 2020; Zhu et al., 2015), and then calculated the average and median values to quantitatively describe the differences in plant traits between Eucalyptus tree and other tree species (Table 2).

Eucalyptus trees have small canopies with the crowns growing at the top of the trunks, resulting in an LAI for Eucalyptus that is usually < 2 m^2/m^2. Other evergreen trees, such as fir and pine, have larger canopies with branches often growing along the trunks, resulting in larger LAI values (typically > 2 m^2/m^2). Eucalyptus leaves live for about 20 months, while fir and pine can have leaf lifespans of over two years up to eight years (Table 2). The shorter leaf lifespan of Eucalyptus results in a larger ratio of new to old leaves in the canopy than the other three evergreen species. According to the leaf litterfall records of these tree species, the leaf litterfall production of these tree species follows a seasonal pattern and peaks in the rainy season (March–June) (Kong et al., 2022), which means that old leaves are shed and new leaves grow during this period. The larger ratio of new to old leaves in the Eucalyptus canopies results in higher red edge and near infrared reflectance, which in turn leads to higher LSWI and EVI values during winter and spring than other evergreen tree species.

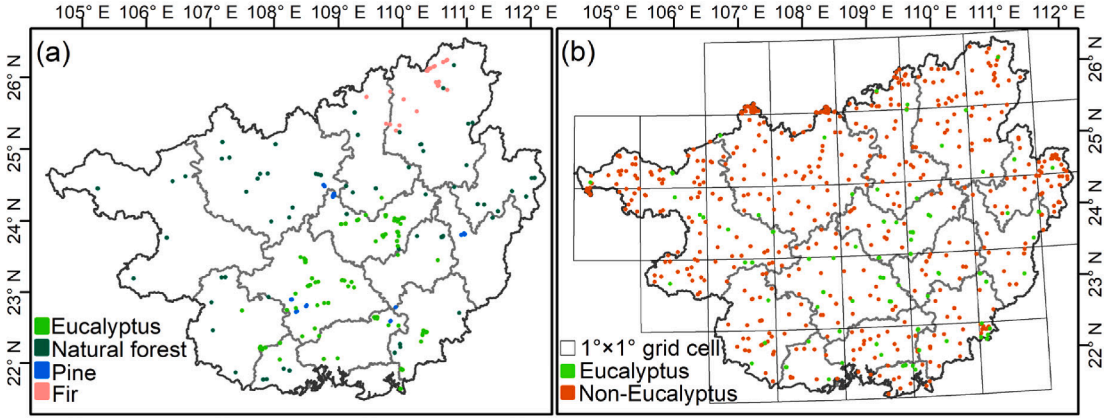

Fig. 5. Spatial distribution of (a) training samples and (b) validation samples for 2020.

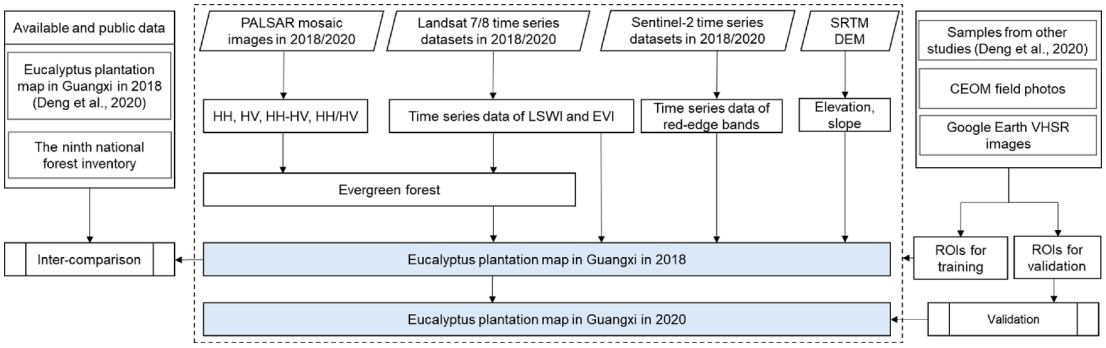

Fig. 6. Flowchart for Eucalyptus plantation mapping.

Table 2
Plant traits for major evergreen tree species in Guangxi. The data were collected from the Plant Trait Database and publications.

		Evergreen broadleaf forest		Evergreen coniferous forest	
		Eucalyptus	Natural evergreen tree	Pine	Fir
Leaf lifespan (month)	Average	20	41	33	87
	Median	21	25	32	96
LAI (m^2/m^2)	Average	1.97	2.52	4.97	4.98
	Median	1.88	2.55	3.85	3.00

Temporal profiles of four Sentinel-2 red edge bands and Landsat/Sentinel-2-based EVI and LSWI were constructed to examine the unique spectral features of Eucalyptus plantations and other evergreen tree species at single pixel level in terms of leaf and plant structure and growth rate (Fig. 7). We found that the seasonal dynamics of red edge bands and vegetation indices of Eucalyptus differed noticeably from those of other evergreen tree species in (1) spring (January to March) and (2) winter (November to December). Eucalyptus plantations had higher values of RE2-4 reflectance in both spring and winter (Fig. 7b–d), which indicates that Eucalyptus plantations have a higher ratio of new to old leaves. In addition, Eucalyptus plantations had higher EVI values in both spring and winter (Fig. 7e), which suggestes that Eucalyptus plantations are more active in the cold season than other evergreen species. These unique phenological characteristics of Eucalyptus plantations are consistent with their plant traits presented in Table 2. Therefore, Eucalyptus plantations can be distinguished from other evergreen tree species in spring and winter.

2.3.3. Algorithm to identify Eucalyptus plantation

To assess the generality of the phenological differences between Eucalyptus and other evergreen tree species in spring and winter (see Section 2.3.2), we overlaid the training samples of Eucalyptus plantations and other evergreen tree species (described in Section 2.2.4) and the phenological metrics for spectral signature analysis. Considering the high correlation between the red edge bands and the greater differences in RE4 between Eucalyptus plantations and other evergreen tree species, we calculated the median values of RE4 and EVI during January to March ($RE4_{spring}$, EVI_{spring}) and November to December ($RE4_{winter}$, EVI_{winter}) (Fig. 8). The histograms showed that a vast majority (over 95 %) of Eucalyptus plantations had $RE4_{spring}$ values of ≥ 0.20, $RE4_{winter}$ values of ≥ 0.25, and EVI_{winter} values of ≥ 0.40 (Fig. 8a, c, d). EVI_{spring} was not as accurate in separating Eucalyptus plantations from other evergreen tree species (Fig. 8b). Eucalyptus plantations in Guangxi are widely distributed in hills and low mountains. Almost all (over 99.5 %) Eucalyptus plantation pixels had DEM ≤ 650 m and slope $< 35°$ (Fig. 9), thus we used DEM ≤ 650 m and slope $< 35°$ as complementary criteria to limit Eucalyptus plantation boundaries. In summary, we developed the algorithm described in Eq. (4) to differentiate Eucalyptus plantations from other evergreen forests.

$$\text{Eucalyptus plantation} = (RE4_{spring} \geq 0.20 \,\&\, RE4_{winter} \geq 0.25 \,\&\, EVI_{winter} \geq 0.40 \,\&\, DEM \leq 650 \,\&\, Slope \leq 35^{\circ}) \quad (4)$$

2.3.4. Accuracy assessment of the resultant Eucalyptus plantation maps

Validation samples from multi-sources were collected for accuracy evaluation. First, we divided the study area into 32 $1^{\circ} \times 1^{\circ}$ grid cells. Twenty random points and square buffers with 60-m by 60-m were generated in each grid cell. Second, we visually checked and interpreted Eucalyptus plantation and non-Eucalyptus plantation samples through overlaying these buffers with VHSR images from Google Earth and Sentinel-2 images in 2020. Field photos from the Global Geo-Referenced Field Photo Library were treated as auxiliary references to cross-reference land cover types. We excluded buffers that did not have explicit land cover information. Finally, 89 Eucalyptus plantation buffer areas (3,515 pixels) and 498 non-Eucalyptus buffer areas (18,760 pixels) (Fig. 5b) were collected for the accuracy assessment of our resultant Eucalyptus map for 2020 by calculating confusion matrices (Foody, 2002).

We also applied the same approach to generate randomly 60-m by 60-m square buffers to collect validation samples for the Eucalyptus and non-Eucalyptus map in 2018. In total, 73 Eucalyptus plantation buffer areas (2,773 pixels) and 475 non-Eucalyptus buffer areas (18,035 pixels) were selected for the validation of the 2018 Eucalyptus map.

2.3.5. Comparison to other datasets of Eucalyptus plantations

We compared the Eucalyptus plantation maps for 2018 derived from our proposed knowledge-based algorithms and Deng et al.'s (2020) study, in terms of accuracy and area estimates. The area comparison was conducted at the provincial and municipal levels.

Since the 1970s, China has established a continuous national forest inventory (NFI) system, with an interval of five years, to study the distribution, composition, quantity, quality, and changes of forest resources in China (Xu et al., 2019). Taking provinces (autonomous regions/municipalities) as the survey units, 415,000 permanent sample sites are reviewed every five years to survey, measure, and record relevant indicators. Forests in NFI include arboreal forest, bamboo forest, and shrub. The Eucalyptus plantation area of Guangxi from the 9th NFI of China in 2015 was used to compare with that of this study in 2018.

3. Results

3.1. Accuracy assessment for the Eucalyptus plantation map in 2020

The confusion matrix (Table 3) for the Eucalyptus plantation map in Guangxi in 2020 was calculated by overlying the validation samples

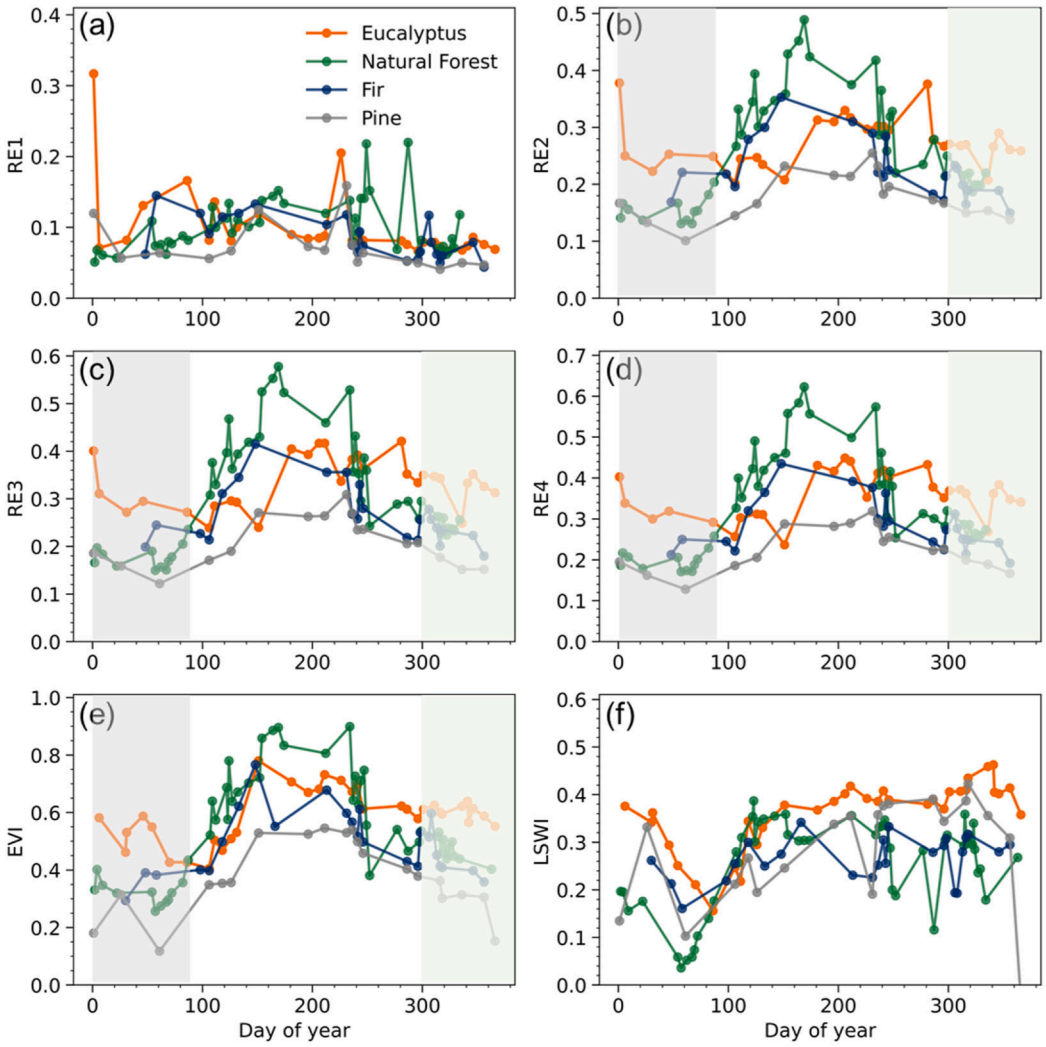

Fig. 7. Time series of (a) RE1, (b) RE2, (c) RE3, (d) RE4, (e) EVI, and (f) LSWI for Eucalyptus plantation, natural forest, pine, and fir in Guangxi. Eucalyptus plantations and other evergreen tree species are evidently different in two typical phenology phases: spring (from January to March, the grey semitransparent boxes) and winter (from November to December, the light green semitransparent boxes).

(Fig. 5b) and the resultant Eucalyptus plantation map. The 2020 Eucalyptus plantation map had a high OA of 0.96. The Eucalyptus plantation had PA and UA of 0.85 and 0.89, and non-Eucalyptus plantation had PA and UA of 0.98 and 0.97, respectively. The Kappa coefficient of the assessment was 0.85, which indicated that our map had a good consistency between the mapped pixels and the ground reference pixels.

Accuracy assessment of Eucalyptus plantation map in 2020 was also carried out by prefecture/city and elevation range (Fig. 10). The PAs of Eucalyptus plantations and OAs were ~0.80 or higher for individual prefectures/cities. The UAs of Eucalyptus plantations were below 0.80 in four cities (Guilin, Liuzhou, Chongzuo, and Qinzhou) and above 0.80 in the ten other prefectures/cities (Fig. 10a). The UAs and OAs of Eucalyptus plantations were $>$ 0.90 in all elevation ranges, slightly higher than PAs ($>$ 0.80) (Fig. 10b). High values of assessment metrics indicated that the resultant 2020 Eucalyptus plantation map had reasonable accuracies.

3.2. Spatial and area distribution of Eucalyptus plantation in Guangxi in 2020

There were approximately 9.37 $\times$ 10^6 ha of forest (Fig. 11a) and 6.96 $\times$ 10^6 ha evergreen forest (Fig. 11b) in 2020, covering 39 % and 29 % of the land area in Guangxi, respectively. The resultant Eucalyptus plantation map estimated the Eucalyptus plantation area of approximately 3.10 $\times$ 10^6 ha (Fig. 11c), which accounted for 45 % of the evergreen forest area. Eucalyptus plantations were mainly located in the central and southern regions of Guangxi. The large blocks of Eucalyptus plantation were under the management of state-owned forestry enterprises, and the small blocks were plantations owned by local farmers and small forestry companies. Among the 14 administrative units, Wuzhou City had the largest Eucalyptus plantation area in Guangxi, followed by Nanning, Baise, and Chongzuo cities. Beihai City had the smallest Eucalyptus plantation area (Table 4). Over half (55 %) of the Eucalyptus plantations were distributed at elevations between 50 m and 300 m, with the area decreasing gradually as elevation increased (Fig. 12a). Moreover, 68 % of the Eucalyptus plantations were located on slopes ranging from 10° to 25°, with the area decreasing as the slope either increases or decreases (Fig. 12b). The distributions of Eucalyptus plantations by elevation and slope (Fig. 12) also demonstrate that the training samples of Eucalyptus plantations (Fig. 9) used in the knowledge-based algorithm development have the representative of the actual distribution of the Eucalyptus plantations.

3.3. Area comparison with other Eucalyptus plantation data

China's 9th NFI (2014–2018) reported that there were 2,560,500 ha

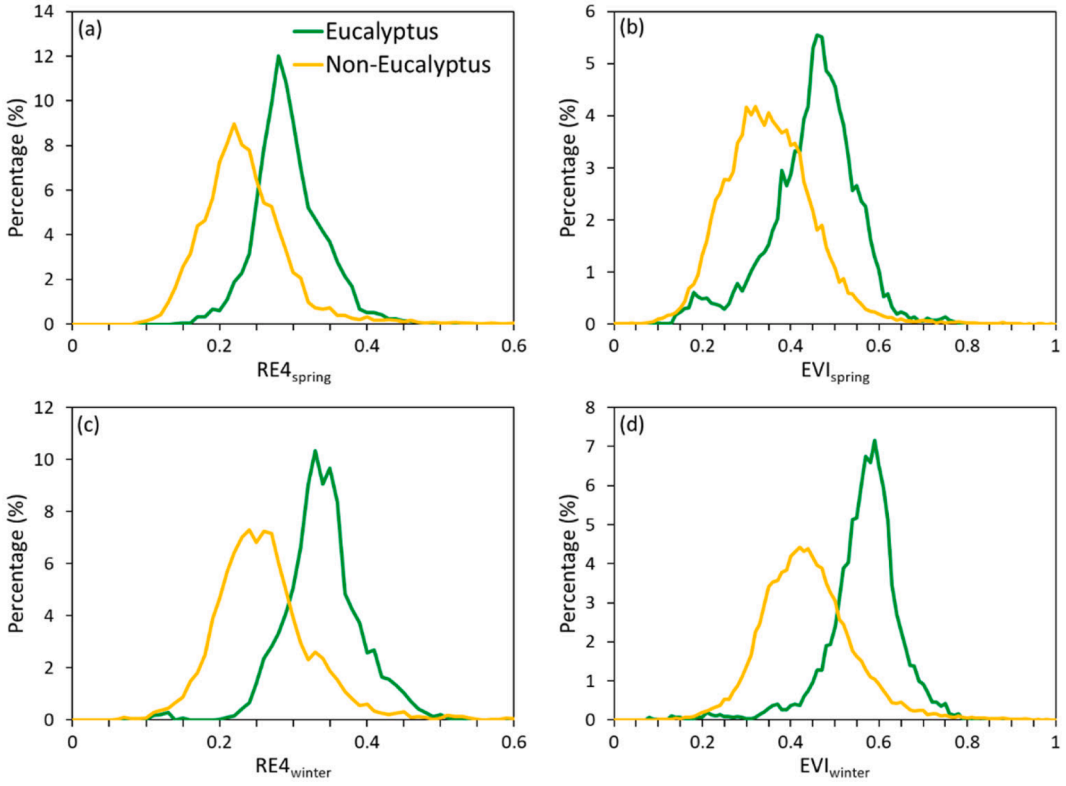

Fig. 8. The histograms of (a) $RE4_{spring}$, (b) EVI_{spring}, (c) $RE4_{winter}$, and (d) EVI_{winter} of Eucalyptus and non-Eucalyptus training samples.

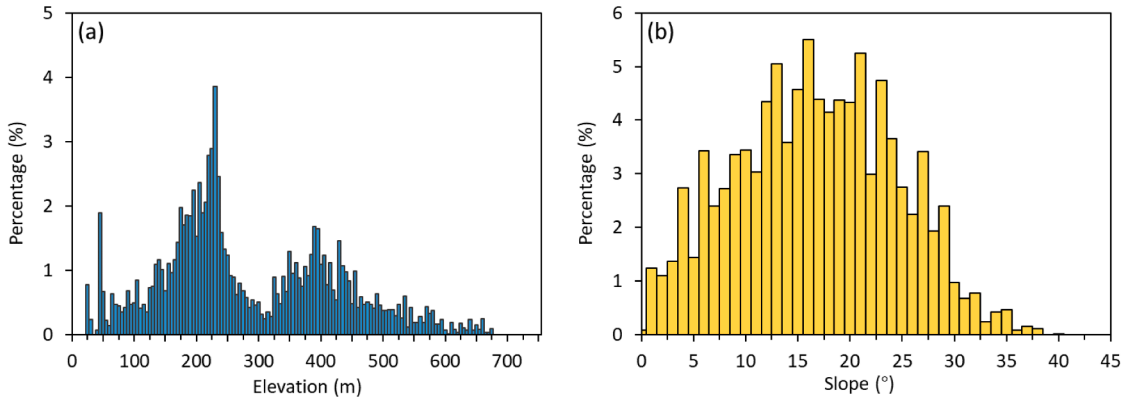

Fig. 9. Distribution of (a) elevation and (b) slope of Eucalyptus plantation training samples.

Table 3
Confusion matrix for the Eucalyptus plantation map in 2020.

		Ground reference		Total	User's accuracy (UA)
		Eucalyptus	Non-Eucalyptus		
Classification	Eucalyptus	2985	371	3356	0.89
	Non-Eucalyptus	530	18,398	18,919	0.97
Total		3515	18,760	22,275	
Producer's accuracy (PA)		0.85	0.98		Overall: 0.96

of Eucalyptus plantations in Guangxi, which was very close to our total (2,567,394 ha in 2018). We also compared the Eucalyptus plantation area estimates for 2018 from our study and Deng et al.'s (2020) study at the provincial and prefecture/city levels. At the provincial level, Eucalyptus plantation area in our dataset is 78 % higher than what Deng et al. (2020) reported (1,439,222 ha). Of the 14 prefectures/cities, we found more Eucalyptus plantation area in 13 municipalities than in Deng et al. (2020) (Fig. 13a). The Pearson's correlation coefficient between these two maps was 0.62 (slope = 0.73, n = 14, $p < 0.05$) (Fig. 13b). We also verified the accuracy of our 2018 Eucalyptus plantation map and compare it with Deng et al.'s (2020) data product for 2018. Our Eucalyptus map had higher OA values (0.96 vs 0.88), as well as higher UA (0.86 vs 0.67) and PA (0.82 vs 0.64) of Eucalyptus plantations than Deng et al.'s (2020) map.

4. Discussion

4.1. The potential of the knowledge-based Eucalyptus plantation mapping algorithm

Guangxi has a complex landscape and a moderate proportion of

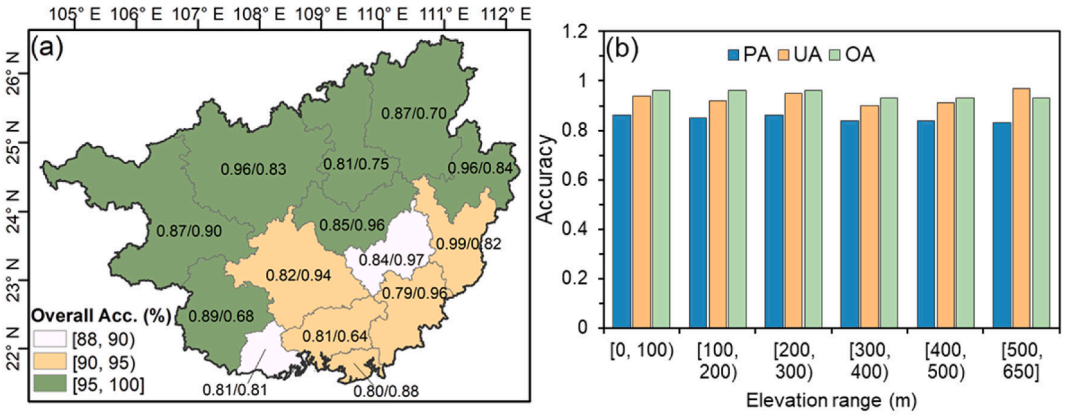

Fig. 10. Accuracy assessment of the Eucalyptus plantation map by (a) prefecture/city and (b) elevation range for 2020. The filling color in (a) indicates the overall accuracy (OA); the labelled text is presented in the format of producer's accuracy (PA)/user's accuracy (UA).

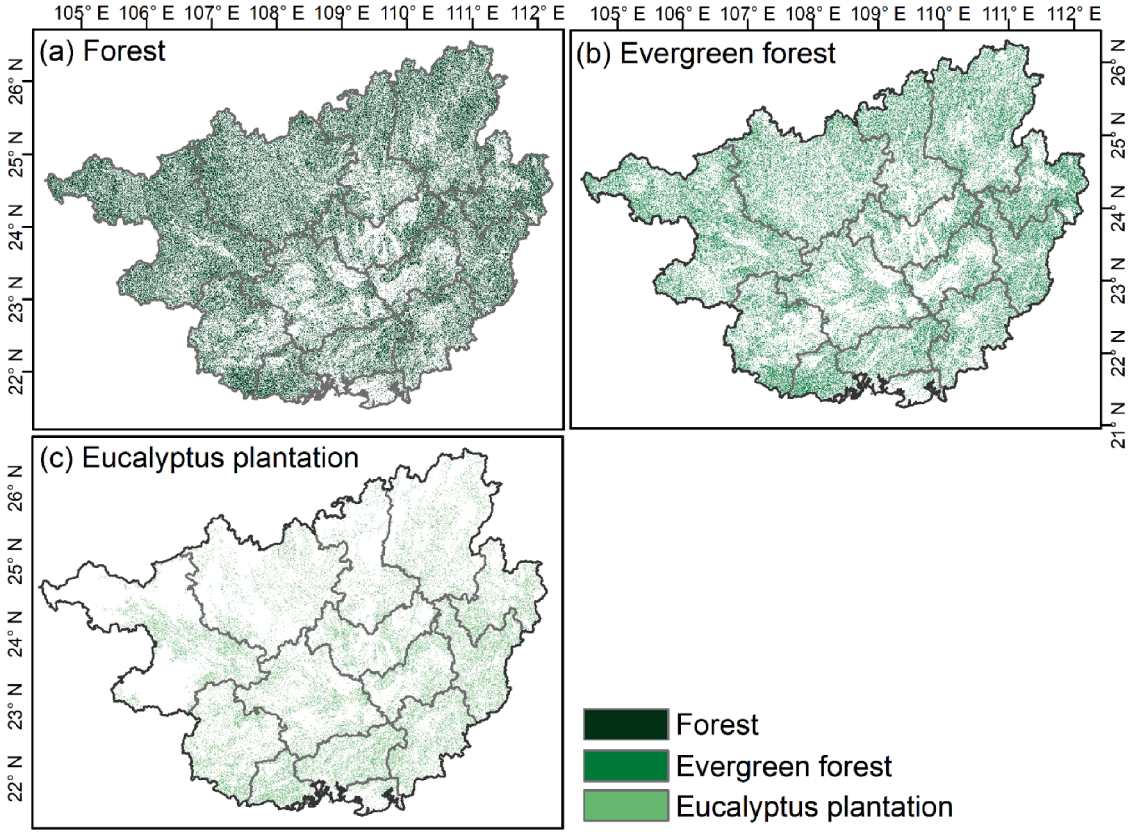

Fig. 11. Spatial distribution of (a) forest, (b) evergreen forest, and (c) Eucalyptus plantation in Guangxi in 2020.

Eucalyptus plantations in Guangxi are managed by local farmers. Time series 30-m Landsat images have been successfully used to map forests and plantations over the last few years (Chen et al., 2017; Dong et al., 2013; Pasquarella et al., 2018). Nevertheless, it is challenging to acquire a sufficient number of high-quality Landsat observations within a year for land cover classification in regions with frequent cloud cover (Griffiths et al., 2019). In this study, we developed a knowledge-based Eucalyptus plantation mapping algorithm by combining PALSAR-2, Sentinel-2, and Landsat images. Landsat and Sentinel-2 time-series data together have a large amount of good-quality observations in a single year, make it possible to better capture phenological information or changes in land surface compared to using a single sensor (Chen et al., 2017; Wang et al., 2020a; Wang et al., 2020b).

Our approach demonstrates the potential of using the red edge bands from Sentinel-2 images to map Eucalyptus plantations on a regional scale. Eucalyptus plantations differ noticeably from other evergreen tree species in terms of red edge bands, particularly over winter and spring seasons (Fig. 7). Many scholars have also emphasized the significance of the red edge bands on tree species classification as they are closely related to chlorophyll content, leaf structure, leaf demography, and canopy structure, which reflect the nature of plant leaves (Immitzer et al., 2016; Peerbhay et al., 2013; Sothe et al., 2017). Compared with other sensors with only a single red edge band, such as RapidEye, the four red edge bands of Sentinel-2 enhance the opportunity to improve the classification of various plantations and other land cover types, as well as retrieval for important biophysical parameters (Clevers and Gitelson, 2013; Forkuor et al., 2018). In Deng et al.'s (2020) study on the Eucalyptus plantation mapping, they combined all four red edge bands

Table 4
Estimated area of forest, evergreen forest, and Eucalyptus plantation by prefecture/city in 2020.

City	Land area (10^6 ha)	Forest area (10^6 ha)	Evergreen forest area (10^6 ha)	Eucalyptus area (10^6 ha)	Percentage of total Eucalyptus area
Guilin	2.77	1.20	0.88	0.24	8 %
Liuzhou	1.86	0.71	0.55	0.14	5 %
Hechi	3.35	1.43	0.95	0.24	8 %
Hezhou	1.18	0.52	0.43	0.21	7 %
Baise	3.62	1.72	1.17	0.29	9 %
Laibin	1.34	0.46	0.34	0.18	6 %
Wuzhou	1.26	0.55	0.48	0.31	10 %
Guigang	1.06	0.33	0.26	0.18	6 %
Nanning	2.21	0.66	0.49	0.31	10 %
Chongzuo	1.73	0.65	0.46	0.28	9 %
Yulin	1.28	0.45	0.37	0.28	9 %
Qinzhou	1.08	0.38	0.32	0.25	8 %
Fangchenggang	0.62	0.25	0.22	0.15	5 %
Beihai	0.40	0.06	0.04	0.04	1 %
Total	23.76	9.37	6.96	3.10	

and NIR bands of Sentinel-2 to distinguish Eucalyptus plantations from pine and fir, by using SVM method. However, it is hard to know how the SVM model made its final decision and how these red edge bands contributed to the identification of Eucalyptus plantations. On the contract, by systematically studying and acquiring knowledge of the unique biophysics of Eucalyptus plantations and their response on satellite images, the knowledge-based algorithm is able to explain the specific role of the red edge bands in Eucalyptus plantation identification, and thus has the potential to be applied directly to other years or regions without the need for large nember of new training samples.

The comparison of Eucalyptus plantation area estimates showed that our Eucalyptus plantation area estimate was substantially higher (78 %) than what Deng et al. (2020) reported (Fig. 13), but our area estimates were very close to the area reported by China's 9th NFI. The Eucalyptus plantation identification strategies and input image data contributed to the inconsistency between our results and those reported by Deng et al. (2020). First, Deng et al. (2020) identified tree plantations by detecting plantation clear-cuts during the harvest cycle, when EVI dropped abruptly after 5 or 6 years. Using time series 3-month median EVI data derived from Landsat 8 between 2013 and 2018, they then separated Eucalyptus plantations from other tree plantations using Sentinel-2 images. Landsat 8 with a 16-day revisit cycle may not provide enough good-quality observations in regions with frequent cloud cover for all three months. Lack of good-quality Landsat images resulted in some Eucalyptus plantation pixels being missed in the plantation identification step.

Second, the reduction of timber harvesting quotas in recent years due to increasingly stringent environmental policies led to a longer rotation cycle of more than five years for Eucalyptus trees in some regions. Eucalyptus pixels in these regions did not meet the 5- or 6-year rotation threshold used in the clear-cut detection algorithm. Third, Deng et al. (2020) used four red edge and NIR bands of Sentinel-2 during the peak growth season (May through September) to delineate Eucalyptus plantations from fir and pine forests. However, we found that the reflectance of all red edge bands in Eucalyptus plantations overlapped with that of fir during the peak growing season (Fig. 7a–d). We also found that the red edge 1 band reflectance was very similar for all tree species (Fig. 7a), but that Eucalyptus plantations had higher red edge reflectance in bands 2, 3, and 4, and higher EVI between November and March (from late fall to winter and early spring seasons) (Fig. 7b–e). Finally, differences in spatial resolutions between our Eucalyptus map (10-m) and Deng et al.'s

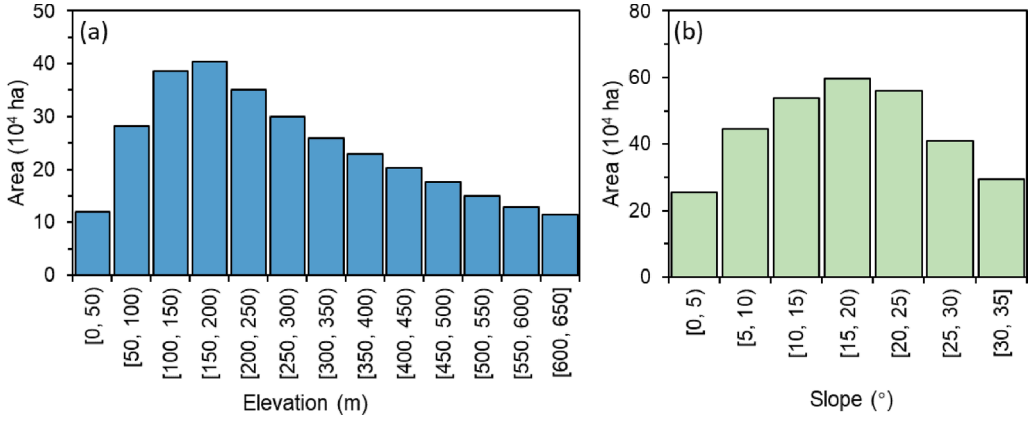

Fig. 12. The histograms for area distribution of Eucalyptus plantations by (a) elevation and (b) slope in 2020.

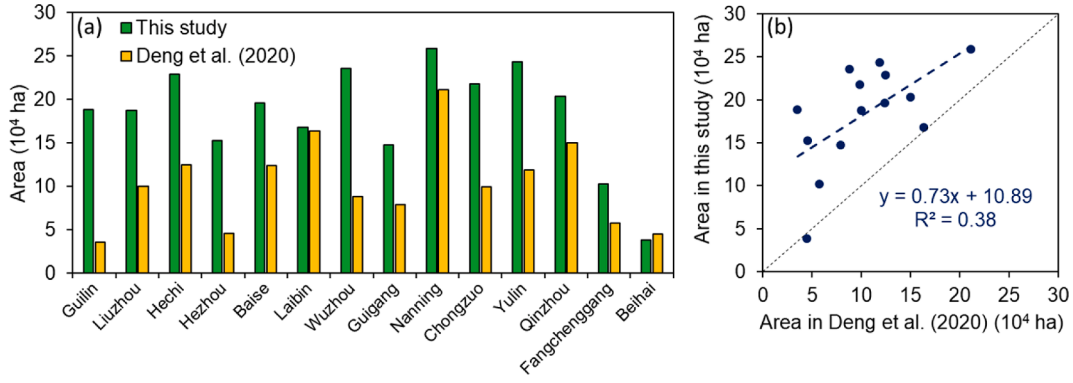

Fig. 13. Comparison of Eucalyptus plantation area in 2018 for Guangxi that we identified in our study and the area reported by Deng et al. (2020).

(2020) dataset (30-m) contributed to the inconsistency in the plantation area estimates to some extent.

4.2. Source of errors in the annual Eucalyptus plantation maps

The accuracy of land cover maps is determined by (1) quality of satellite observations, (2) *in-situ* observations, (3) mapping algorithms, (4) the temporal and spatial resolutions of satellite data, and (5) land cover classification schemes and definitions (Foody, 2002). The Eucalyptus plantation maps derived from this study also have various error sources and limitations.

Frequent cloud and rain in Guangxi limit the number of good-quality optical observations in some regions, although we have combined all available Landsat 7/8 and Sentinel-2 images. In our study, over 99.99 % of pixels in 2020 had 10 or more good-quality observations when using both Sentinel-2 and Landsat7/8 imagery (Fig. 4c, d). Thus, the data were frequent enough to use our frequency-based algorithm to map evergreen forest (Wang et al., 2020b). However, 12.61 % of pixels had less than two good-quality Sentinel-2 observations in certain phenology-important months (January through March), which was mainly located in the northeast Guangxi (Fig. 14a). Insufficient good-quality observations may lead to failure to capture differences between Eucalyptus and other tree species.

We utilized three phenology/spectral variables ($RE4_{spring}$, $RE4_{winter}$, and EVI_{winter}) and two topography variables (elevation and slope) to build the algorithm for mapping Eucalyptus plantations. To evaluate the significance of the individual variables, we conducted a sensitivity analysis by comparing the changes of producer's, user's and overall accuracies of the Eucalyptus plantation maps derived from the full model (all the five variables; EP_map), and from the partial models by removing one variable at a time, $RE4_{spring}$ (EP_w/o_$RE4_{SP}$), $RE4_{winter}$ (EP_w/o_$RE4_{WI}$), EVI_{winter} (EP_w/o_EVI_{WI}), DEM (EP_w/o_DEM), and slope (EP_w/o_slope) (Fig. 15). The results indicated that all the five variables play a crucial role in improving user's accuracy and reducing the commission errors in Eucalyptus plantation maps (Fig. 15). Therefore, the quality and quantity of images during these two specific periods (January to March, November to December) may contribute to the error and uncertainty in the resultant Eucalyptus plantation maps.

There are many small patches of Eucalyptus trees planted by local farmers, which inevitably introduces mixed pixels in 30-m Landsat images and 25-m PALSAR-2 images, and this may cause slight underestimation in Eucalyptus plantation area. Also, young and newly planted Eucalyptus plantations may be omitted because of differences in their spectral signatures from mature Eucalyptus plantations (Benedek and Szirányi, 2009). Although Eucalyptus trees can reach over 5-m in the first year (Zeng et al., 2015), which would satisfy the minimum tree height in the FAO forest definition, young and newly planted Eucalyptus plantations have a small canopy and are mostly surrounded by bare land. Thus, the canopy cover can be < 10 %, which might bring uncertainty in Eucalyptus identification. Combining Google Earth VHSR images and field surveys to identify the young and newly planted Eucalyptus plantations can be considered in the design of future studies.

Our knowledge-based Eucalyptus plantation mapping algorithm was designed to distinguish Eucalyptus plantations from natural evergreen trees and coniferous trees. Howecer, our approach might be complicated by bamboo, an evergreen perennial plant, which is also extensively distributed in Guangxi. According to China's 9th NFI, Moso bamboo forest is the main species of bamboo forest in China, accounting for 72.96 % of the total bamboo area (Xu et al., 2019). Moso bamboo forest covered an area of 163,300 ha in Guangxi, with a primary distribution in northeast Guangxi (Qi et al., 2022). Due to the lack of field surveys of bamboo forest and the difficulty of identifying bamboo by visually checking Google Earth VHSR images, we did not consider bamboo forests in Eucalyptus plantation mapping algorithm development. As bamboo has a much higher LAI (≥ 3 m^2/m^2) than Eucalyptus (Huang et al., 2021b; Ji et al., 2021; Li et al., 2021), it may have low red edge reflectance, similar to natural evergreen and coniferous trees. Nevertheless, the applicability of our Eucalyptus mapping algorithm in regions with a lot of bamboo forests still needs to be assessed with field surveys in the near future.

4.3. Implications and future development of Eucalyptus plantation mapping algorithm

Our Eucalyptus plantation maps for Guangxi, China at 10-m spatial resolution advance our understanding on the area and spatial distribution of Eucalyptus plantations and provide important information for Eucalyptus planning and management. Our knowledge-based Eucalyptus mapping algorithm allows for monitoring Eucalyptus plantation dynamics over Sentinel-2 data record. The Eucalyptus plantation classification criteria we developed were derived from the unique phenological features of Eucalyptus plantations. Within a specific region, environmental variables such as terrain, climatology, cultivation and management practices for Eucalyptus plantation are relatively stable across time. Thus, there is promise for using our Eucalyptus plantation mapping method to map Eucalyptus plantations in other years. Also, the proposed knowledge-based mapping method could potentially to map Eucalyptus plantations in other regions and even globally by adjusting thresholds of phenology variables with local training samples. These adjustments can resolve potential differences in the phenology indicators of Eucalyptus plantations among various environmental conditions. In addition, our Eucalyptus plantation classification approach would be useful for distinguishing coniferous and broadleaf forests (Fig. 7) or for detecting other tree species by exploring the unique phenological features of plant traits and revising the phenology metrics.

The improvement in Eucalyptus plantation mapping contains two aspects. In terms of input data, the frequent cloud cover in the tropics is a major error source. There are two strategies for reducing errors caused by poor-quality observations. First, we can integrate optical images with comparable spatial resolution to Sentinel-2 data to increase the amount

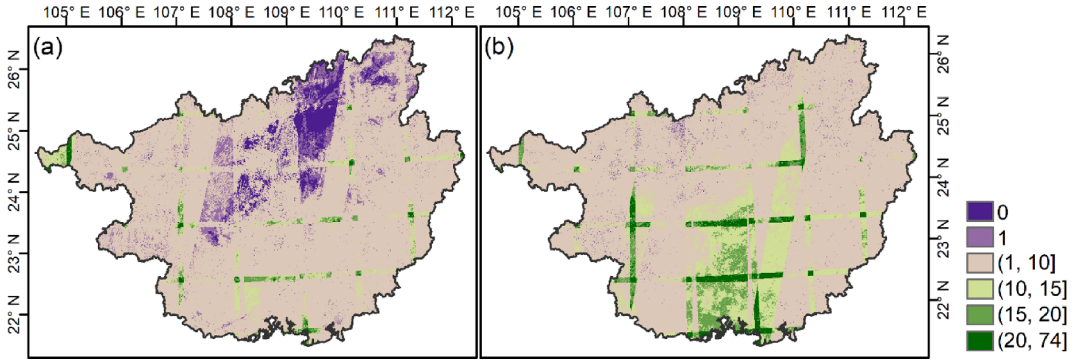

Fig. 14. Amount of good-quality Sentinel-2 observations in (a) spring (January to March) and (b) winter (November to December).

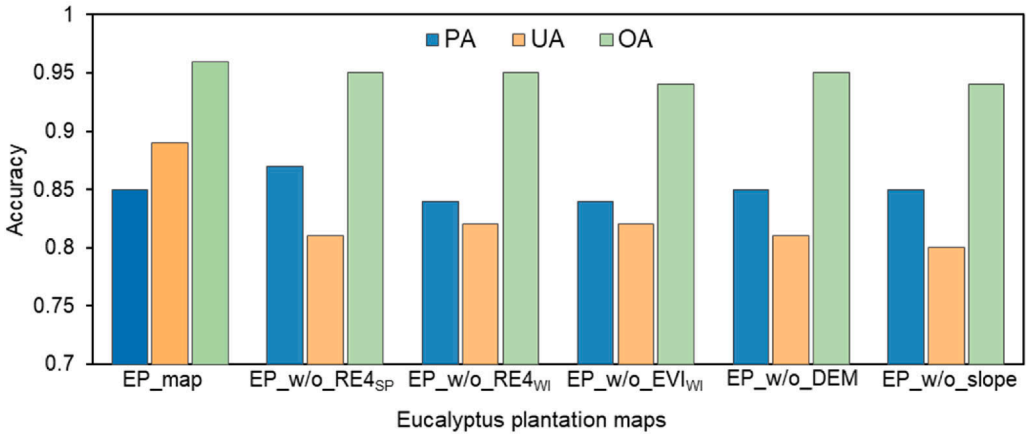

Fig. 15. Sensitivity analysis of parameters for the Eucalyptus plantation mapping. The producer's accuracy (PA), user's accuracy (UA), and overall accuracy (OA) are used as indicators to compare the resultant Eucalyptus plantation map (EP_map) and the Eucalyptus plantation maps without $RE4_{spring}$ (EP_w/o_$RE4_{SP}$), $RE4_{winter}$ (EP_w/o_$RE4_{WI}$), EVI_{winter} (EP_w/o_EVI_{WI}), DEM (EP_w/o_DEM), and slope (EP_w/o_slope).

of good-quality images, such as Worldview-3, which has great potential for land use and land cover classification (Chen et al., 2019; Xian et al., 2019). Second, we can combine weather-independent microwave images, such as Sentinel-1, with optical to override the constraints posed by cloud coverage. C-band Sentinel-1 satellite can penetrate part of the tree canopy, but mainly captures information on top-of-canopy features, and has the potential to distinguish between different types of leaves. Incorporating microwave data may also improve the optical-only classification of Eucalyptus plantation. With respect to classification features, in addition to red edge bands and EVI, we can also combine red edge indices such as red edge spectral indices (RESI), which can also contain information on the structure of vegetation and have been proven useful in plantation classification (Xiao et al., 2020). Additionally, several studies have incorporated textural features into plantation mapping approaches (Chen et al., 2021; Zhang et al., 2020a), so we can also investigate the use of textural features in the future work.

5. Conclusions

Here, we proposed a knowledge-based algorithm to identify and generate annual maps of Eucalyptus plantations in Guangxi at 10-m spatial resolution by combining PALSAR-2, Landsat, and Sentinel-2 in a single year. Our approach produced a Eucalyptus plantation map for 2020 with high overall, producer's, and user's accuracies and Kappa coefficient, which were higher than previous mapping efforts. Our knowledge-based mapping algorithm highlights the potential of Sentinel-2 red edge bands for tree species classification and rapid mapping of Eucalyptus plantations at large scales using multiple satellite data, and our resultant 10-m spatial resolution Eucalyptus plantation maps provide vital information for sustainable Eucalyptus plantation planning and management as well as ecological assessment conservation.

CRediT authorship contribution statement

Chenchen Zhang: Conceptualization, Methodology, Software, Validation, Visualization, Writing – original draft, Writing – review & editing. **Xiangming Xiao:** Conceptualization, Methodology, Writing – review & editing, Supervision, Project administration, Funding acquisition. **Liangcheng Zhao:** Methodology, Writing – review & editing. **Yuanwei Qin:** Methodology, Writing – review & editing. **Russell Doughty:** Writing – review & editing. **Xinxin Wang:** Writing – review & editing. **Jinwei Dong:** Writing – review & editing. **Xuebin Yang:** Writing – review & editing.

Declaration of Competing Interest

The authors declare that they have no known competing financial interests or personal relationships that could have appeared to influence the work reported in this paper.

Data availability

Data will be made available on request.

Acknowledgement

This study was supported in part by grants from the U.S. National Science Foundation (1911955, 1946093). The publication fee was provided in part by the University of Oklahoma Libraries' Open Access Fund. We thank the editors and reviewers for their time and effort in the review of our manuscript, and their comments and suggestions helped us to improve the manuscript.

References

Benedek, C., Szirányi, T., 2009. Change detection in optical aerial images by a multilayer conditional mixed Markov model. IEEE Trans. Geosci. Remote Sens. 4 (7), 3416–3430.
Chen, W., Li, X., Wang, L., 2019. Fine land cover classification in an open pit mining area using optimized support vector machine and worldview-3 imagery. Remote Sens. 12, 82.
Chen, Y., Peng, Z., Ye, Y., Jiang, X., Lu, D., Chen, E., 2021. Exploring a uniform procedure to map Eucalyptus plantations based on fused medium–high spatial resolution satellite images. Int. J. Appl. Earth Obs. Geoinf. 103, 102462.
Chen, B., Xiao, X., Li, X., Pan, L., Doughty, R., Ma, J., Dong, J., Qin, Y., Zhao, B., Wu, Z., 2017. A mangrove forest map of China in 2015: Analysis of time series Landsat 7/8 and Sentinel-1A imagery in google earth engine cloud computing platform. ISPRS J. Photogramm. Remote Sens. 131, 104–120.
Clevers, J.G., Gitelson, A.A., 2013. Remote estimation of crop and grass chlorophyll and nitrogen content using red-edge bands on Sentinel-2 and-3. Int. J. Appl. Earth Obs. Geoinf. 23, 344–351.
Clevers, J.G., Kooistra, L., 2011. Using hyperspectral remote sensing data for retrieving canopy chlorophyll and nitrogen content. IEEE J. Sel. Top. Appl. Earth Obs. Remote Sens. 5, 574–583.
da Costa, L.B., de Carvalho, O.L.F., de Albuquerque, A.O., Gomes, R.A.T., Guimarães, R. F., de Carvalho Júnior, O.A., 2021. Deep semantic segmentation for detecting eucalyptus planted forests in the Brazilian territory using sentinel-2 imagery. Geocarto Int. 1–13.
Danylo, O., Pirker, J., Lemoine, G., Ceccherini, G., See, L., McCallum, I., Kraxner, F., Achard, F., Fritz, S., 2021. A map of the extent and year of detection of oil palm plantations in Indonesia, Malaysia and Thailand. Sci. Data. 8, 1–8.
De Luca, G., Silva, J.M.N., Di Fazio, S., Modica, G., 2022. Integrated use of Sentinel-1 and Sentinel-2 data and open-source machine learning algorithms for land cover mapping in a Mediterranean region. Eur. J. Remote Sens. 55, 52–70.
DeFries, R.S., Townshend, J., 1994. NDVI-derived land cover classifications at a global scale. Int. J. Remote Sens. 15, 3567–3586.

Deng, X., Guo, S., Sun, L., Chen, J., 2020. Identification of short-rotation eucalyptus plantation at large scale using multi-satellite imageries and cloud computing platform. Remote Sens. 12, 2153.
DeRose, R.J., Seymour, R.S., 2010. Patterns of leaf area index during stand development in even-aged balsam fir–red spruce stands. Canadian J. Forest Res. 40, 629–637.
Dong, R., Li, W., Fu, H., Gan, L., Yu, L., Zheng, J., Xia, M., 2020. Oil palm plantation mapping from high-resolution remote sensing images using deep learning. Int. J. Remote Sens. 41, 2022–2046.
Dong, J., Xiao, X., Sheldon, S., Biradar, C., Duong, N.D., Hazarika, M., 2012a. A comparison of forest cover maps in Mainland Southeast Asia from multiple sources: PALSAR, MERIS, MODIS and FRA. Remote Sens. Environ. 127, 60–73.
Dong, J., Xiao, X., Sheldon, S., Biradar, C., Xie, G., 2012b. Mapping tropical forests and rubber plantations in complex landscapes by integrating PALSAR and MODIS imagery. ISPRS J. Photogramm. Remote Sens. 74, 20–33.
Dong, J., Xiao, X., Chen, B., Torbick, N., Jin, C., Zhang, G., Biradar, C., 2013. Mapping deciduous rubber plantations through integration of PALSAR and multi-temporal Landsat imagery. Remote Sens. Environ. 134, 392–402.
Dong, J., Xiao, X., Kou, W., Qin, Y., Zhang, G., Li, L., Jin, C., Zhou, Y., Wang, J., Biradar, C., 2015. Tracking the dynamics of paddy rice planting area in 1986–2010 through time series Landsat images and phenology-based algorithms. Remote Sens. Environ. 160, 99–113.
Dong, J., Xiao, X., Menarguez, M.A., Zhang, G., Qin, Y., Thau, D., Biradar, C., Moore III, B., 2016. Mapping paddy rice planting area in northeastern Asia with Landsat 8 images, phenology-based algorithm and google earth engine. Remote Sens. Environ. 185, 142–154.
FAO, 2020. Global Forest Resources Assessment 2020 – Key findings. Rome. https://doi.org/10.4060/ca8753en.
Foody, G.M., 2002. Status of land cover classification accuracy assessment. Remote Sens. Environ. 80, 185–201.
Forestry Bureau of Guangxi, 2018. In: The Planning and Development of Guangxi Forestry Industry in the 13th Five-Year..
Forkuor, G., Dimobe, K., Serme, I., Tondoh, J.E., 2018. Landsat-8 vs. Sentinel-2: examining the added value of sentinel-2's red-edge bands to land-use and land-cover mapping in Burkina Faso. GIsci. Remote Sens. 55, 331–354.
Forrester, D.I., Bauhus, J., Cowie, A.L., Vanclay, J.K., 2006. Mixed-species plantations of Eucalyptus with nitrogen-fixing trees: a review. For. Ecol. Manag. 233, 211–230.
Forstmaier, A., Shekhar, A., Chen, J., 2020. Mapping of eucalyptus in Natura 2000 areas using Sentinel 2 imagery and artificial neural networks. Remote Sens. 12, 2176.
Griffiths, P., Nendel, C., Hostert, P., 2019. Intra-annual reflectance composites from Sentinel-2 and Landsat for national-scale crop and land cover mapping. Remote Sens. Environ. 220, 135–151.
Hansen, M.C., Potapov, P.V., Moore, R., Hancher, M., Turubanova, S.A., Tyukavina, A., Thau, D., Stehman, S.V., Goetz, S.J., Loveland, T.R., 2013. High-resolution global maps of 21st-century forest cover change. Sci. 342, 850–853.
Huang, F., Fan, W., Du, H., Xu, X., Wu, J., Zheng, M., Du, Y., 2021b. Estimation of Leaf Area Index of Moso Bamboo Canopies. J. Sustain. For. 1–16.
Huang, C., Zhang, C., Liu, Q., Li, H., Yang, X., Liu, G., 2021a. Multi-Feature classification of optical and SAR remote sensing images for typical tropical plantation species. Sci. Sil. Sin. 57, 80–91.
Huete, A., Liu, H., Batchily, K., Van Leeuwen, W., 1997. A comparison of vegetation indices over a global set of TM images for EOS-MODIS. Remote Sens. Environ. 59, 440–451.
Huete, A., Didan, K., Miura, T., Rodriguez, E.P., Gao, X., Ferreira, L.G., 2002. Overview of the radiometric and biophysical performance of the MODIS vegetation indices. Remote Sens. Environ. 83, 195–213.
Imhoff, M.L., 1995. A theoretical analysis of the effect of forest structure on synthetic aperture radar backscatter and the remote sensing of biomass. IEEE Trans. Geosci. Remote Sens. 33, 341–351.
Immitzer, M., Vuolo, F., Atzberger, C., 2016. First experience with Sentinel-2 data for crop and tree species classifications in central Europe. Remote Sens. 8, 166.
Ji, J., Li, X., Du, H., Mao, F., Fan, W., Xu, Y., Huang, Z., Wang, J., Kang, F., 2021. Multiscale leaf area index assimilation for Moso bamboo forest based on Sentinel-2 and MODIS data. Int. J. Appl. Earth Obs. Geoinf. 104, 102519.
Kong, J., Lin, Y., Huang, F., Liu, W., He, Q., Su, Y., Li, J., Wang, G., Qiu, Q., 2022. Effects of Fertilization and Dry-Season Irrigation on Litterfall Dynamics and Decomposition Processes in Subtropical Eucalyptus Plantations. Front. Ecol. Evol. 10, 919571.
Kovacs, J., Lu, X., Flores-Verdugo, F., Zhang, C., de Santiago, F.F., Jiao, X., 2013. Applications of ALOS PALSAR for monitoring biophysical parameters of a degraded black mangrove (Avicennia germinans) forest. ISPRS J. Photogramm. Remote Sens. 82, 102–111.
Le Maire, G., Dupuy, S., Nouvellon, Y., Loos, R.A., Hakamada, R., 2014. Mapping short-rotation plantations at regional scale using MODIS time series: Case of eucalypt plantations in Brazil. Remote Sens. Environ. 152, 136–149.
Li, X., Du, H., Zhou, G., Mao, F., Zheng, J., Liu, H., Huang, Z., He, S., 2021. Spatiotemporal dynamics in assimilated-LAI phenology and its impact on subtropical bamboo forest productivity. Int. J. Appl. Earth Obs. Geoinf. 96, 102267.
Li, L., Li, N., Lu, D., Chen, Y., 2019. Mapping Moso bamboo forest and its on-year and off-year distribution in a subtropical region using time-series Sentinel-2 and Landsat 8 data. Remote Sens. Environ. 231, 111265.
Liang, W., Liu, J., Chen, Q., Chen, X., Zhong, S., 2017. A comparison of object-oriented methods of extracting eucalyptus information based on GF-2 images. For. Res. Manag 54–59.
Lu, X., Huang, Y., Yan, H., Wei, W., Li, Z., 2020. Research on eucalyptus extraction based on automatic threshold decision tree classification. For. Res. Manag. 4, 117–126.
Mthembu, S.L., 2001. Estimating leaf area index (LAI) of gum tree (Eucalyptus grandis X camaldulensis) using remote sensing imagery and LiCor-2000 [University of Natal].
Nomura, K., Mitchard, E.T., 2018. More than meets the eye: Using Sentinel-2 to map small plantations in complex forest landscapes. Remote Sens. 10, 1693.
Oliveira, D., Martins, L., Mora, A., Damásio, C., Caetano, M., Fonseca, J., Ribeiro, R.A., 2021. Data fusion approach for eucalyptus trees identification. Int. J. Remote Sens. 42, 4087–4109.
Parida, B.R., Kumar, P., 2020. Mapping and dynamic analysis of mangrove forest during 2009–2019 using landsat–5 and sentinel–2 satellite data along Odisha Coast. Trop. Ecol. 61, 538–549.
Pasquarella, V.J., Holden, C.E., Woodcock, C.E., 2018. Improved mapping of forest type using spectral-temporal Landsat features. Remote Sens. Environ. 210, 193–207.
Peerbhay, K.Y., Mutanga, O., Ismail, R., 2013. Investigating the capability of few strategically placed Worldview-2 multispectral bands to discriminate forest species in KwaZulu-Natal, South Africa. IEEE J. Sel. Top. Appl. Earth Obs. Remote Sens. 7, 307–316.
Qi, S., Song, B., Liu, C., Gong, P., Luo, J., Zhang, M., Xiong, T., 2022. Bamboo forest mapping in China using the dense Landsat 8 image archive and google earth engine. Remote Sens. 14, 762.
Qin, Y., Xiao, X., Dong, J., Zhang, G., Shimada, M., Liu, J., Li, C., Kou, W., Moore III, B., 2015. Forest cover maps of China in 2010 from multiple approaches and data sources: PALSAR, Landsat, MODIS, FRA, and NFI. ISPRS J. Photogramm. Remote Sens. 109, 1–16.
Reiche, J., Lucas, R., Mitchell, A.L., Verbesselt, J., Hoekman, D.H., Haarpaintner, J., Kellndorfer, J.M., Rosenqvist, A., Lehmann, E.A., Woodcock, C.E., 2016. Combining satellite data for better tropical forest monitoring. Nat. Clim. Change. 6, 120–122.
Rodríguez, A.C., D'Aronco, S., Schindler, K., Wegner, J.D., 2021. Mapping oil palm density at country scale: An active learning approach. Remote Sens. Environ. 261, 112479.
Rody, Y.P., Ribeiro, A., Pezzopane, J.E.M., Gleriani, J.M., Almeida, A.Q., Leite, F.P., 2014. Estimates of the leaf area index (LAI) using LAI-2000 and hemispherical photos in Eucalyptus plantations. Ciência Florestal 24, 925–934.
Shimada, M., Isoguchi, O., Tadono, T., Isono, K., 2009. PALSAR radiometric and geometric calibration. IEEE Trans. Geosci. Remote Sens. 47, 3915–3932.
Shimada, M., Itoh, T., Motooka, T., Watanabe, M., Shiraishi, T., Thapa, R., Lucas, R., 2014. New global forest/non-forest maps from ALOS PALSAR data (2007–2010). Remote Sens. Environ. 155, 13–31.
Sothe, C., Almeida, C.M.d., Liesenberg, V., Schimalski, M.B., 2017. Evaluating Sentinel-2 and Landsat-8 data to map sucessional forest stages in a subtropical forest in Southern Brazil. Remote Sens. 9, 838.
Tucker, C.J., 1979. Red and photographic infrared linear combinations for monitoring vegetation. Remote Sens. Environ. 8, 127–150.
Wang, J., Xiao, X., Liu, L., Wu, X., Qin, Y., Steiner, J.L., Dong, J., 2020a. Mapping sugarcane plantation dynamics in Guangxi, China, by time series Sentinel-1, Sentinel-2 and Landsat images. Remote Sens. Environ. 247, 111951.
Wang, X., Xiao, X., Zou, Z., Hou, L., Qin, Y., Dong, J., Doughty, R.B., Chen, B., Zhang, X., Chen, Y., 2020b. Mapping coastal wetlands of China using time series Landsat images in 2018 and Google Earth Engine ISPRS. J. Photogramm. Remote Sens. 163, 312–326.
Wang, M., Zheng, Y., Huang, C., Meng, R., Pang, Y., Jia, W., Zhou, J., Huang, Z., Fang, L., Zhao, F., 2022. Assessing Landsat-8 and Sentinel-2 spectral-temporal features for mapping tree species of northern plantation forests in Heilongjiang Province, China. For. Ecosyst. 9, 100032.
White, D.A., Ren, S., Mendham, D.S., Balocchi-Contreras, F., Silberstein, R.P., Meason, D., Iroumé, A., Ramirez de Arellano, P., 2022. Is the reputation of Eucalyptus plantations for using more water than Pinus plantations justified? Hydrol. Earth Syst. Sci. 26, 5357–5371.
Xian, G., Shi, H., Dewitz, J., Wu, Z., 2019. Performances of WorldView 3, Sentinel 2, and Landsat 8 data in mapping impervious surface. Remote Sens. Appl.: Soc. Environ. 15, 100246.
Xiao, X., Hollinger, D., Aber, J., Goltz, M., Davidson, E.A., Zhang, Q., Moore III, B., 2004. Satellite-based modeling of gross primary production in an evergreen needleleaf forest. Remote Sens. Environ. 89, 519–534.
Xiao, X., Boles, S., Liu, J., Zhuang, D., Frolking, S., Li, C., Salas, W., Moore III, B., 2005a. Mapping paddy rice agriculture in southern China using multi-temporal MODIS images. Remote Sens. Environ. 95, 480–492.
Xiao, X., Boles, S., Frolking, S., Li, C., Babu, J.Y., Salas, W., Moore III, B., 2006. Mapping paddy rice agriculture in South and Southeast Asia using multi-temporal MODIS images. Remote Sens. Environ. 100, 95–113.
Xiao, X., Biradar, C.M., Czarnecki, C., Alabi, T., Keller, M., 2009. A simple algorithm for large-scale mapping of evergreen forests in tropical America. Africa and Asia. Remote Sens. 1, 355–374.
Xiao, C., Li, P., Feng, Z., Liu, Y., Zhang, X., 2020. Sentinel-2 red-edge spectral indices (RESI) suitability for mapping rubber boom in Luang Namtha Province, northern Lao PDR. Int. J. Appl. Earth Obs. Geoinf. 93, 102176.
Xiao, X., Zhang, Q., Hollinger, D., Aber, J., Moore III, B., 2005b. Modeling gross primary production of an evergreen needleleaf forest using MODIS and climate data. Ecol. Appl. 15, 954–969.
Xu, J., Xie, S., Han, A., Rao, R., Huang, G., Chen, X., Hu, J., Liu, Q., Yang, X., Zhang, L., 2019. Forest resources in China—The 9th national forest inventory. National Forestry and Grassland Administration.
Yan, Z., Zhou, Q., Teng, M., Ji, H., Zhang, J., He, W., Ye, Y., Wang, B., Wang, P., 2019. High planting density and leaf area index of masson pine forest reduce crown transmittance of photosynthetically active radiation. Glob. Ecol. Conserv. 20, e00759.
Yang, X., Xiao, X., Qin, Y., Wang, J., Neal, K., 2021. Mapping forest in the southern Great plains with ALOS-2 PALSAR-2 and Landsat 7/8 data. Int. J. Appl. Earth Obs. Geoinf. 104, 102578.

Zeng, W., Tomppo, E., Healey, S.P., Gadow, K.V., 2015. The national forest inventory in China: history-results-international context. For. Ecosyst. 2, 1–16.
Zhang, C., Huang, C., Li, H., Liu, Q., Li, J., Bridhikitti, A., Liu, G., 2020a. Effect of textural features in remote sensed data on rubber plantation extraction at different levels of spatial resolution. Forests 11, 399.
Zhang, Y., Wang, X., 2021. Geographical spatial distribution and productivity dynamic change of eucalyptus plantations in China. Sci. Rep. 11 (1), 19764.
Zhang, X., Xiao, X., Wang, X., Xu, X., Chen, B., Wang, J., Ma, J., Zhao, B., Li, B., 2020b. Quantifying expansion and removal of Spartina alterniflora on Chongming island, China, using time series Landsat images during 1995–2018. Remote Sens. Environ. 247, 111916.
Zhao, Y., Chen, X., Smallman, T.L., Flack-Prain, S., Milodowski, D.T., Williams, M., 2020. Characterizing the error and bias of remotely sensed LAI products: An example for tropical and subtropical evergreen forests in South China. Remote Sens. 12, 3122.
Zhu, J., Pan, Z., Wang, H., Huang, P., Sun, J., Qin, F., Liu, Z., 2019. An improved multi-temporal and multi-feature tea plantation identification method using Sentinel-2 imagery. Sensors 19, 2087.
Zhu, L., Zhao, P., Wang, Q., Ni, G., Niu, J., Zhao, X., Zhang, Z., Zhao, P., Gao, J., Huang, Y., 2015. Stomatal and hydraulic conductance and water use in a eucalypt plantation in Guangxi, southern China. Agric. For. Meteorol. 202, 61–68.
Zinn, Y.L., Resck, D.V., da Silva, J.E., 2002. Soil organic carbon as affected by afforestation with Eucalyptus and Pinus in the Cerrado region of Brazil. For. Ecol. Manag. 166, 285–294.